Thermally stimulated third-order optical nonlinearity in Cd-doped CuO–PVA thin films under cw laser illumination

Y. S. Tamgadge[1] · V. G. Pahurkar[2] · S. S. Talwatkar[3] · A. L. Sunatkari[4] · G. G. Muley[2]

Abstract We report synthesis, linear and third-order nonlinear optical properties of Cd-doped CuO–PVA nanocomposite thin films. Cd-doped CuO nanoparticles (NPs) were obtained by chemical synthesis method, and spin coating technique was used to obtain thin films in polyvinyl alcohol matrix. X-ray diffraction (XRD) shows formation of crystalline CuO having monoclinic phase with average particle size of 10 nm. Ultraviolet–visible (UV–Vis) spectroscopy attests formation of NPs by witnessing strong blue shift in the excitonic absorption. Absorption wavelength of CuO NPs shifts from 365 to 342 nm for Cd doping of 1–5 wt%. Both XRD and UV–Vis data confirm decrease in particle size with increase in Cd-doping concentration. Thin films have been characterized by Z-scan technique under continuous-wave He–Ne laser, and enhanced values of nonlinear refractive index n_2 and nonlinear absorption coefficient β have been obtained. Enhancements in the nonlinear optical properties have been attributed to the thermal effect due to strong linear absorption coefficient combined with increased thermo-optic coefficient. Contributing mechanisms such as photoacoustic effect, surface states effect and dielectric effect due to dopant and thin film structure have been discussed.

1 Introduction

Nanostructured materials offer great advantages over bulk materials owing to enhanced properties due to high surface-to-volume ratio and quantum size effects. Semiconducting nanomaterials are known to have peculiar shape and size-dependent physical, chemical, electrical and optical properties which can be engineered as per application requirements [1]. These nanomaterials are widely used in optoelectronics, electronics, medicine, photonics, etc. [2–4]. Third-order nonlinearity in semiconducting materials is gaining extreme importance because of its potential applications in optical switching, optical limiters, optoelectronic devices, optical signal processing, optical waveguides, ultrafast optical communication systems, optical storage systems, ultrafast nonlinear optical (NLO) devices, etc. [5]. Various sensors and optical detectors are being developed and used for scientific and industrial applications. Most of them use high-intense lasers for their active operation and may cause damage if exposed to lasers for long duration. In order to protect such devices from high-intense laser beams, need of optical limiters is also evident. Optical limiters are basically NLO materials which work on the principle of intensity-dependent refractive and absorptive properties that result into NLO effects such as self-focusing, self-defocusing, saturable absorption and reverse saturable absorption [6]. Such NLO materials can serve the purpose of passive optical limiters which perform the job of optical limiting without the requirement of any additional switches or controlling circuits [7]. Most of the NLO properties of different materials are studied with picosecond

✉ G. G. Muley
gajananggm@yahoo.co.in

1   Department of Physics, Mahatma Fule Arts, Commerce and SRC Science College, Warud, Amravati District 444906, MH, India

2   Department of Physics, Sant Gadge Baba Amravati University, Amravati 444602, MH, India

3   Department of Physics, D K Marathe and N G Acharya College, Chembur, Mumbai 440071, MH, India

4   Department of Physics, Siddharth College of Arts, Science and Commerce, Fort, Mumbai 440001, MH, India

and nanosecond laser pulses for their applications in ultra-fast devices, optical switching, etc. However, in most of the area, continuous-wave (cw) laser is used, and in this regime, NLO properties of the materials are also important for their possible applications in sensor protecting devices.

Metal oxide nanoparticles (NPs) have attracted great attention due to their tunable optical, electronic, magnetic and catalytic properties [8]. Nanocrystalline CuO semiconductor is one of the best promising materials as it has potential applications in optics and optoelectronics. Copper oxide is an excellent nanoparticles system for investigating the size-induced structural transformations and phase stability. Copper oxide has two phases, i.e., cuprous oxide (Cu_2O) and cupric oxide (CuO). CuO is a p-type semiconductor having direct bulk energy gap of about 1.85 eV [9] at room temperature. The effect of doping on properties of CuO nanostructures is being studied widely for many practical applications such as an efficient catalytic agent, gas-sensing material, lithium batteries, solar cells, optical switches and magnetic storage media [10–14]. The NLO response of thin films is of particular interest because of its application in integrated NLO devices [15]. Nanocomposite materials consisting of two or more phases are known to show enhanced third-order NLO susceptibility due to dielectric effect, quantum confinement and surface states effect [16]. L-Arginine has already been used as a capping agent for the synthesis of nanoparticles [17–19]. To the best of our knowledge, there are no reports on the investigations of third-order NLO properties of Cd-doped CuO NPs embedded in polymer matrix. Composite materials containing CuO and polyvinyl alcohol (PVA) exhibit the merits of blending, processability, flexibility and easy thin film-forming properties. Such material designs are assumed to show excellent NLO properties, especially related to optical limiting properties. With this aim, we present here the detailed investigations on third-order NLO properties of *Cd–CuO–PVA* nanocomposite thin films by Z-scan technique under low-power cw laser illumination. We synthesized Cd-doped CuO nanoparticles (NPs) by using L-arginine as capping agent. Thin films of Cd-doped CuO NPs with PVA have been prepared using spin coating technique. CuO NPs and thin films have been characterized by various techniques, and results are presented here.

2 Materials and methods

Undoped and Cd-doped CuO nanoparticles were synthesized by wet chemical method, and thin films with PVA were prepared using spin coating technique. All chemicals of analytical reagent grade were used as received without further purification. Copper (II) chloride dihydrate ($CuCl_2·2H_2O$, 99.99 %), sodium hydroxide pellets (NaOH, 99 %) and ethanol were procured from SD Fine Chemicals,

Mumbai. Cadmium chloride monohydrate ($CdCl_2·H_2O$, 99.99 %) was purchased from LOBA Chemie, India. L-Arginine and PVA (99.99 %, M.W. 10000) were purchased from Sigma-Aldrich, USA. Stock solutions of 1 M $CuCl_2·2H_2O$, 2 M NaOH and 1 M L-arginine in double-distilled water were prepared. Initially, CuO nanoparticles were synthesized using L-arginine as capping agent (sample CLR3). For this, 4 ml stock solution of $CuCl_2·2H_2O$ was added into 100 ml double-distilled water and stirred continuously for 1 h under constant heating at 100 °C. The temperature was maintained above 100 °C throughout the reaction. Three milliliter of L-arginine from stock solution was added drop wise into blue-colored copper chloride solution. The resultant solution was again stirred for another 30 min. After this, NaOH stock solution was added drop wise into this solution. The color of the solution changes to black immediately, and large amount of L-arginine arrested CuO NPs in the form of black precipitate were obtained. The precipitate then centrifuged at 4000 rpm (R-4C, REMI, India) for 20 min and washed 2–3 times with double-distilled water. The precipitate was then dried for 24 h in hot air electric oven. For the synthesis of Cd-doped CuO NPs, appropriate amount of $CdCl_2·H_2O$ amounting to 1 wt% (CCD1), 2 wt% (CCD2) and 5 wt% Cd (CCD5) have been added into copper chloride solution before the addition of L-arginine. By following similar steps, black precipitate of Cd-doped CuO NPs was obtained. For the preparation of composite thin film, synthesized undoped and Cd-doped CuO NPs were dispersed in double-distilled water separately and ultrasonicated for 10 h to achieve good stable suspensions. Solution of PVA was also prepared and mixed, amounting 10 wt%, with suspensions of pure and doped CuO nanoparticles. The solutions were stirred for 1 h, ultrasonicated for another 2 h and were used to prepare thin films on good optical quality glass slides using spin coating technique. Thin films were dried in hot air oven and were used for characterization. Thickness of thin films was measured by ellipsometric method on Sentech ellipsometer (model no.: SEN research SE 850 DUV Variable angle), Germany. Table 1 shows average thickness of thin films of undoped and Cd-doped CuO–PVA nanocomposites.

All samples of CuO NPs were subjected to structural and morphological characterization by X-ray diffraction

**Table 1** Undoped and Cd-doped CuO–PVA nanocomposite thin films

Sample code	Nanocomposite details	Film thickness (nm)
CLP	CLR3 0.1 mM + 10 wt% PVA	199
CC1P	CCD1 0.1 mM + 10 wt% PVA	218
CC2P	CCD2 0.1 mM + 10 wt% PVA	221
CC5P	CCD5 0.1 mM + 10 wt% PVA	214

(XRD) using Rigaku diffractometer Miniflex II with nickel-filtered CuK$_\alpha$ radiation (λ = 1.5406 Å); transmission electron microscopy (TEM) using JEM-2100 HR-TEM, Make-JEOL, Japan; field emission scanning electron microscopy (FESEM), Hitachi S-4800, Japan; and energy-dispersive X-ray absorption spectroscopy (EDX) using scanning electron microscope JSM-7000F, JEOL, Japan. Ultraviolet–visible (UV–Vis) spectroscopy was performed using UV–visible spectrophotometer (BLK-C-SR, Stellar-Net, USA) in the wavelength range 190–900 nm. Fourier transform infrared (FTIR) spectra were recorded using IR double-beam spectrophotometer, 8400S, Shimadzu, Japan. Open- and closed-aperture Z-scan technique, as developed by Bahae et al. [20, 21], was utilized to characterize samples for third-order optical nonlinearity.

3 Results and discussion

3.1 Optical studies using UV–Vis and FTIR spectroscopy

Figure 1 shows absorption spectra and variations of $(\alpha h\nu)^2$ versus photon energy ($h\nu$) for L-arginine-passivated Cd-doped CuO NPs samples. All samples show broad excitonic absorption in the wavelength range 330–565 nm due to inter-band surface states transitions in CuO NPs [22]. In the crystal of semiconductor, electron in conduction band and hole in valence band has columbic interaction to create excitons. In nanoscale, motion of these excitons is highly constrained that results into size-dependent novel optical properties. From figure, it can be seen that the maximum absorption takes place at 365, 350 and 342 nm for the samples CCD1, CCD2 and CCD5, respectively. Blue shifting of the maximum absorption wavelength is thus obvious. CuO NPs doped with highest concentration Cd shows strong blue shift, and reduced particle sizes are obtained as indicated by quantum confinement effect [23, 24]. However, absorption intensity goes on decreasing, and absorption bands become narrow as particle size decreases. This indicates that L-arginine effectively modified the surface of CuO NPs by annealing surface states. Low density of surface states might have caused less and selective absorption. The optical band gap (E_g) of CuO nanoparticles is calculated using the equation $\alpha = A^*(E_g - h\nu)^n/h\nu$, where α is absorption coefficient (the absorption coefficient α has been calculated using the relation: $\alpha = 2.303 \log[1/(1-A)]/d$, where 'A' is absorbance and 'd' is thickness of the sample), E_g is band gap, A^* is constant and n is equal to 1/2 for direct transition and 2 for indirect transitions [25]. The band gap energy E_g is obtained by extrapolating the linear portion of the plot to the energy axis. Blue shift in
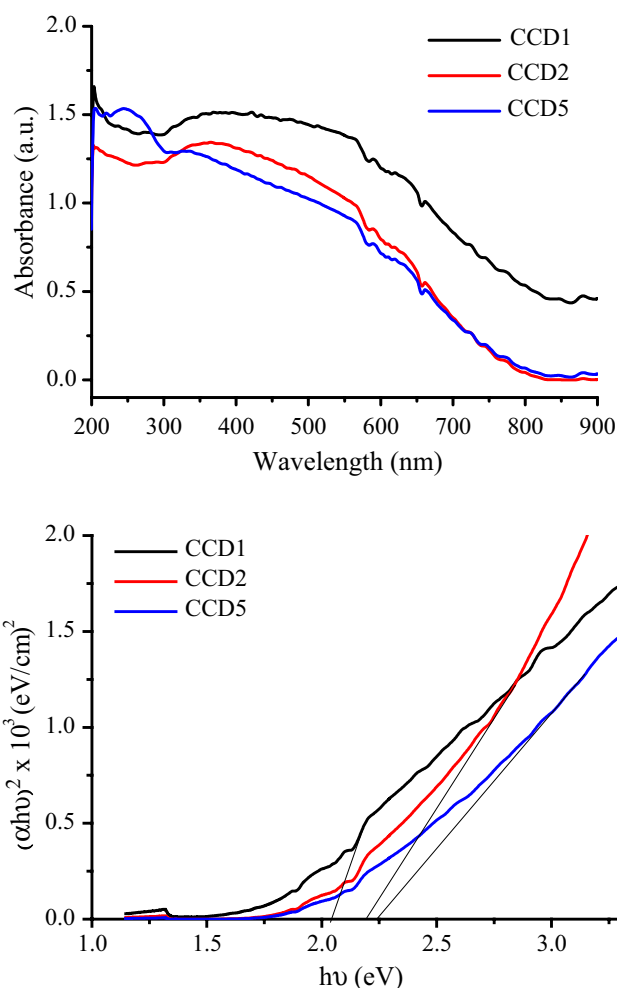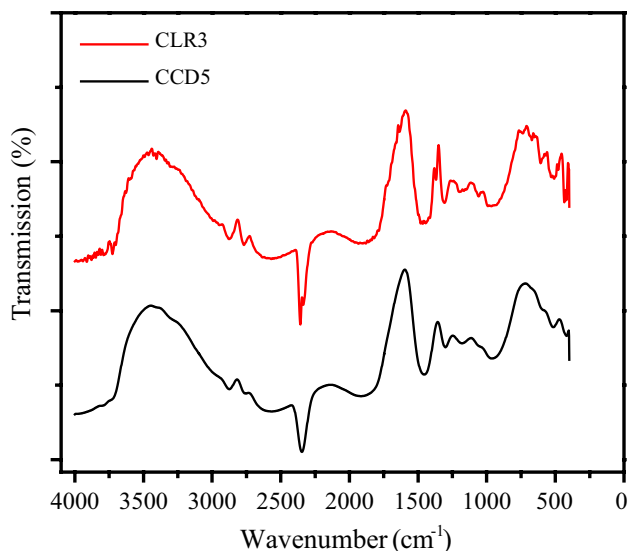

Fig. 1 Absorption spectra and optical band gap analysis of CuO NPs

the optical band gaps has been observed as the particle size decreases for highest concentration of dopant. As obtained particle size for CuO NPs is in the range of Bohr exciton radius which is 6.6–28.7 nm [23], this regime is treated as strong confinement regime [26]. The energies of the possible optical transitions can be obtained through the relation $E_n = E_g - E_{exc} + (\hbar^2\pi^2n^2/2MR^2)$, where $M (= m_e^* + m_h^*)$ is the total mass of the e–h pair, R is radius of nanoparticle, E_g is bulk band gap energy, E_{exc} is the exciton binding energy and n is the quantum number [27]. The particle size for all samples is calculated from UV–Vis spectra by using effective mass approximation (EMA) [28]. The EMA formula can be stated as: $E_g = E_{bulk} + h^2/8r^2[(1/m_e^*) + (1/m_h^*)] - e^2/4\pi\varepsilon_0\varepsilon_r\gamma_e$, where E_g is band gap energy of NPs, E_{bulk} is energy gap for bulk semiconductor (=1.85 eV for bulk CuO [9]), m_e^* and m_h^* are effective electron mass (0.65 m_e) and effective hole mass (1.75 m_e), respectively, γ_e is Bohr exciton radius, ε_r is relative dielectric constant (7.11), ε_0 is dielectric constant of
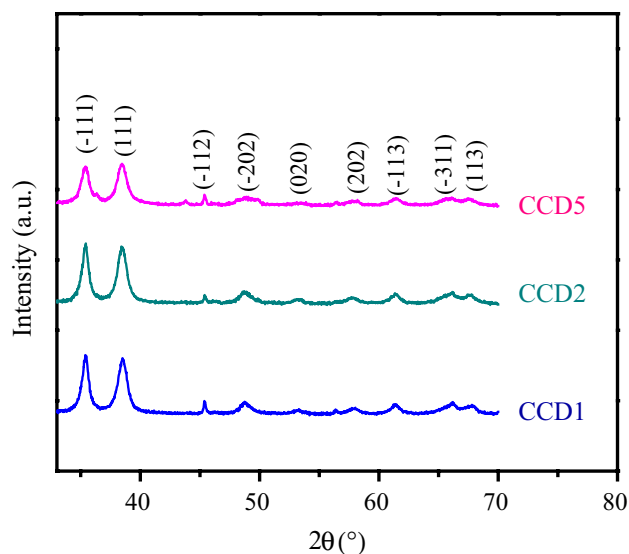
Table 2 Particle size and optical band gap of CuO NPs

Sample	Particle size (nm)			Energy gap (eV)
	XRD	EMA model	TEM	
CLR3	12	9	–	2.51
CCD1	11	7	–	2.05
CCD2	10	6	–	2.19
CCD5	8	5	7	2.25

Fig. 2 FTIR spectrum of L-arginine-capped CuO NPs

Fig. 3 XRD pattern of undoped and Cd-doped CuO NPs

3.2 Structural and morphological studies using XRD, TEM, FESEM and EDX

Figure 3 shows XRD spectra for undoped and Cd-doped CuO NPs. All the d values corresponding to the XRD peaks show the presence of a monoclinic end-centered phase of crystalline CuO with cell parameters $a = 4.6927$ Å, $b = 3.4283$ Å and $c = 5.1370$ Å, $\alpha = \gamma = 90^{\circ}$ and $\beta = 99.55^{\circ}$ which is in good agreement with the reported values (JCPDS card no. 80-1916). Peak broadening confirms the nanocrystalline nature of CuO crystals [33]. The intensity of peaks has not been significantly changed with increasing concentration of Cd in CuO, which indicates that the crystallinity of the particles is retained. The peaks corresponding to the metallic Cd/CdO have not been detected in XRD. This suggests that Cd has been doped into the lattice at Cu lattice sites. Considering the spherical nature, particle size of these nanoparticles is calculated by Debye–Scherrer formula, $d = k\lambda/(\beta \cos\theta)$, where k is a constant ($k = 0.93$) and β is width of the diffraction peak at half maxima. The average crystallite size calculated for (-111), (111) and (-202) planes was found to be 11, 10 and 8 nm for 1, 2 and 5 wt% Cd-doped CuO NPs samples. This is the average particle size, and different crystallites may have different sizes for different samples. Particle size of Cd-doped CuO NPs was found to decrease with increase in the concentration of Cd dopant. The role of L-arginine is also evident for Cd-doped CuO NPs as all passivated NPs possess smaller particle size. Table 2 shows particle size of all Cd-doped CuO NPs calculated using various characterizations and also the optical band gap calculated using UV–Vis spectra.
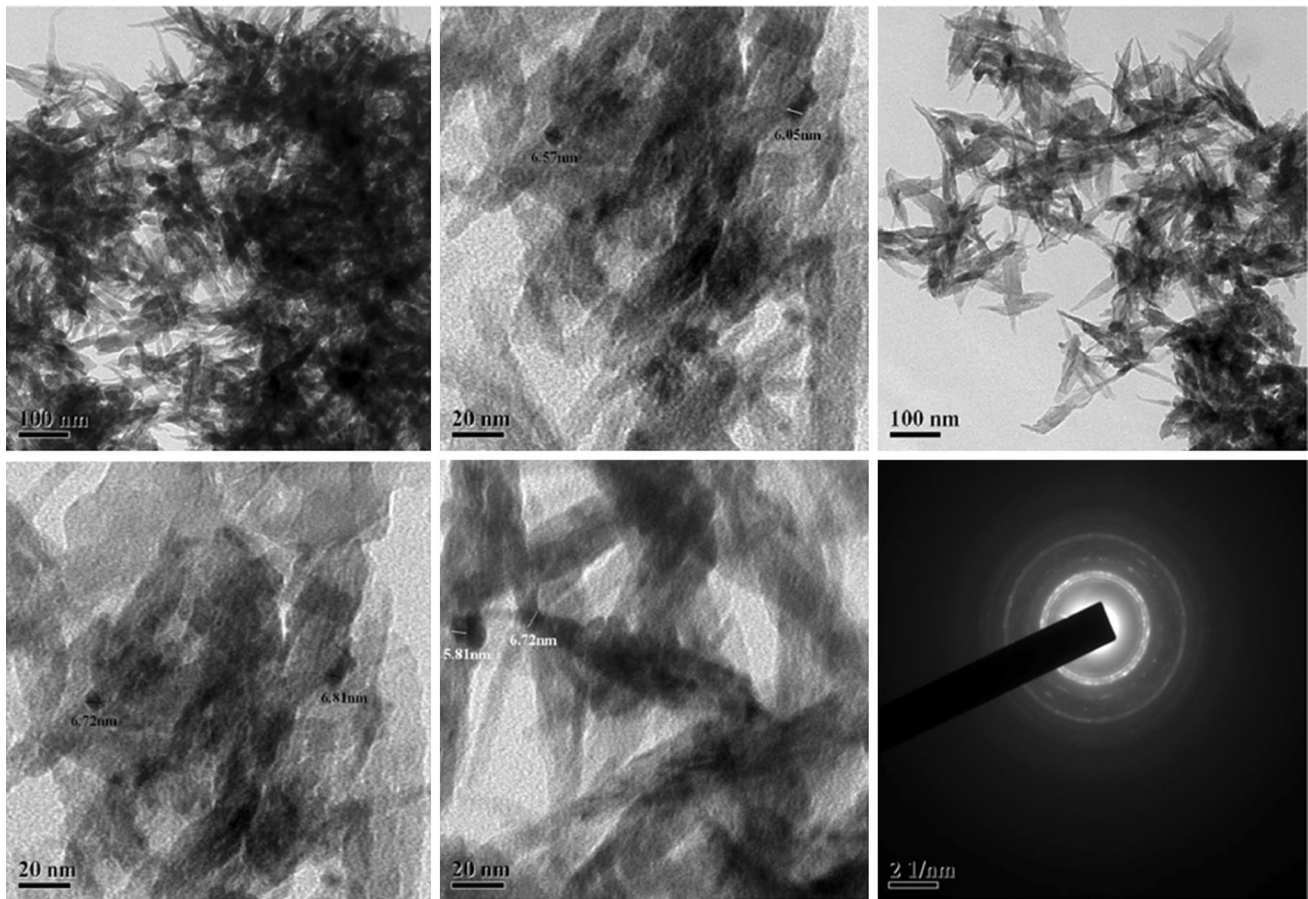
vacuum and r is the radius of NPs. Particle sizes calculated and band gaps determined from Fig. 1 are listed in Table 2.

The functional groups and bonding structure of copper oxide (CuO) NPs capped with L-arginine (sample name CLR3) and doped with Cd (sample name CCD5) were investigated by FTIR spectroscopy. Figure 2 shows FTIR spectra of synthesized CuO NPs capped with L-arginine and CuO NPs doped with Cd. The broad absorption band from 2331 to 2880 cm^{-1} may be attributed to symmetric and asymmetric stretching of O–H and C–H bonding. Peak at 1700 cm^{-1} is due to asymmetric C=O stretching, and strong peak at 1504 cm^{-1} is due to C–H stretching. The peaks at 1404 and 1330 cm^{-1} can be attributed to symmetric stretching vibrations of COO$^-$ group. Peak at 1042 cm^{-1} is due to C–O bonding, and C–H bonding gives peak at 948 cm^{-1}. COO$^-$ bonding again gives peak at 669 cm^{-1}, and torsional modes of CNH$_2$ generate peak at 518 cm^{-1}. All these peaks confirm the presence of L-arginine [29]. The presence of CuO may be confirmed by peaks at 590, 530 and 470 cm^{-1} [30–32]. IR signature of Cd has not been identified in the present spectrum as the dopant percentage is very low.

Fig. 4 TEM micrographs of 5 wt% Cd-doped CuO NPs

Figure 4 depicts TEM micrographs and SAED pattern of 5 wt% Cd-doped CuO NPs taken at various magnifications. Micrographs clearly attest formation of CuO NPs with uniform near spherical structure. Few micrographs show agglomeration of CuO NPs which may be due to excess quantity of nanopowder taken at the time of sample preparation and less ultrasonication. TEM data show that CuO NPs with average particle size of 7 nm have been obtained. This result is in good agreement with XRD and UV–Vis data.

Figure 5a, b depicts FESEM images of 5 wt% Cd-doped CuO–PVA nanocomposite thin film. Images show that Cd-doped CuO NPs have been uniformly dispersed in PVA matrix. All doped CuO NPs have uniform morphology, and their shape and size are retained in the polymer matrix. PVA thus acts as good host matrix for the dispersion of CuO NPs. Figure 6 shows EDX spectra for the sample of 5 wt% Cd-doped CuO NPs. The spectrum indicates the presence of only Cu, O and Cd which confirms the purity of prepared samples and doping is confirmed.

3.3 Z-scan study

Nonlinear refraction coefficient n_2, nonlinear absorption coefficient β and third-order optical nonlinear susceptibility $\chi^{(3)}$ have been determined using closed-aperture and open-aperture Z-scan technique described and developed by Bahae et al. [34]. The intensity-dependent nonlinear refraction is expressed by the relation.

$$n(I) = n_0 + n_2 I \tag{1}$$

where n_0 is the linear refractive index, n_2 is the nonlinear refractive index and I is the intensity of the laser beam.

For a third-order NLO process where nonlinear absorption can be neglected, the nonlinear refractive index n_2 can be deduced from the empirical relation between the induced phase distortion and change in transmittance ($\Delta\phi_0$ and ΔT_{pv}) [20, 21].
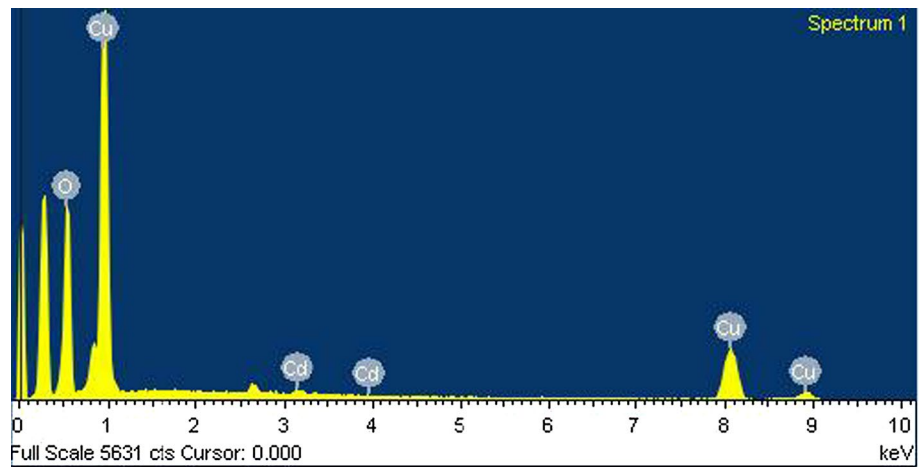
$$\Delta T_{pv} = 0.406(1 - S)^{0.27}\Delta\phi_0 \tag{2}$$

$$\Delta\phi_0 = \frac{2\pi}{\lambda}n_2 I_0 L_{eff} \tag{3}$$
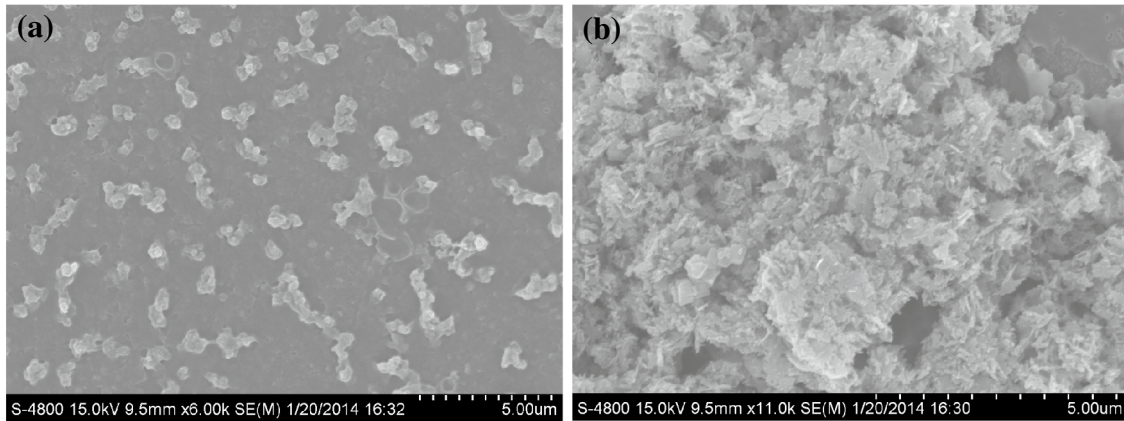
Fig. 5 FESEM micrographs of 5 wt% Cd-doped CuO–PVA nanocomposite thin film

Fig. 6 EDX spectra of 5 wt% Cd-doped CuO NPs

$$n_2 = \frac{\Delta T_{pv}}{k I_0 L_{eff} 0.406(1-S)^{0.27}} \qquad (4)$$

where ΔT_{pv} is change in transmittance between peak and valley, $\Delta\phi_0$ is induced phase distortion, S is transmittance through aperture, L_{eff} is effective thickness of sample ($L_{eff} = \frac{1-\exp(-\alpha L)}{\alpha}$, α is linear absorption coefficient and L is measured thickness of sample) and I_0 is peak intensity at the focus.

Nonlinear absorption coefficient β can be evaluated using following relation.

$$T(z, S=1) = \sum_{m=0}^{\infty} \frac{[-q_0(z)]^m}{(m+1)^{3/2}} \quad for \quad |q_0(0)|\langle 1 \qquad (5)$$

where $q_0(z) = \beta I_0 L_{eff}/(1 + z^2/z_0^2)$, $z_0 = \frac{k\omega_0^2}{2}$ is Rayleigh's range and ω_0 is beam waist.

When laser light falls on optically nonlinear medium (weakly absorbing), part of light is absorbed by the medium and the medium expands due to heating. This expansion travels in radial direction in the form of acoustic disturbances. Due to this, temperature and density gradients are induced within the medium that change the refractive index of the medium. This effect is called the thermal lensing effect [35]. This effect highly depends on the time scales of the incident laser light. It can be said that, when we use the cw laser (where pulse duration is much longer than acoustic propagation time), index change is proportion to change in density of the liquid. In liquid media, density variation is important; however, in solid thin films, density variation is very low (and can be taken as constant), and index change is primarily due to change in temperature. In this regime, the index change is governed by thermal diffusion [7]. The use of a cw laser in Z-scan experiments leads to the determination of the thermo-optic effect that is associated with the dependence of the linear refractive index and absorption coefficient with temperature (T):

$$n = n_0 + (\mathrm{d}n/\mathrm{d}T)\Delta T(n, r) \qquad (6)$$

where r is the spatial position, which is relevant to a Gaussian beam. The optical absorption at 632.8 nm may trigger a progressive increase in the absorption. This will lead to the formation of a thermal lens that will be the dominant contribution in the results of the Z-scan experiments [36].

The thermo-optic coefficient ($\mathrm{d}n/\mathrm{d}T$) can be evaluated from the expression: [34]

$$n_2 = (\mathrm{d}n/\mathrm{d}T)\alpha\omega_0^2/4\kappa \qquad (7)$$

where κ is the thermal conductivity ($\kappa = (\rho C_p)D$, ρ is density of the medium, C_p is specific heat at constant pressure and D is thermal diffusivity).

Using obtained values of n_2 and β, real and imaginary parts of NLO susceptibility and effective NLO susceptibility can be obtained from following relations

$$\mathrm{Re}\left[\chi^{(3)}\right] = 10^{-4}\frac{\varepsilon_0 n_o^2 c^2}{\pi}n_2\,(\mathrm{cm}^2/\mathrm{W})$$

$$\mathrm{Im}\left[\chi^{(3)}\right] = 10^{-2}\frac{\varepsilon_0 n_o^2 c^2\lambda}{4\pi^2}\beta\;(\mathrm{cm}/\mathrm{W}) \qquad (8)$$

$$\chi^{(3)} = \left[\left(\mathrm{Re}\left[\chi^{(3)}\right]\right)^2 + \left(\mathrm{Im}\left[\chi^{(3)}\right]\right)^2\right]^{1/2}$$

In order to study nonlinear refraction, thin film samples of nanocomposite were subjected to closed-aperture Z scan, and value of linear aperture transmittance was kept at 0.4 ($S = 0.4$). Pure nonlinear refractive contribution is extracted by dividing closed-aperture data by open-aperture data [20, 21]. Figure 7 shows closed-aperture Z-scan profiles for all samples which exhibit pre-focal transmittance maximum followed by post-focal transmittance minimum (i.e., peak and valley configuration). This configuration is associated with negative value of n_2 and shows self-defocusing effect [20, 21]. It is observed that the value of nonlinear refractive index n_2 increases with the increase in the doping concentration of Cd in CuO and attains maximum value for 5 wt% Cd doping. The physical origin of this large value of n_2 is attributed to the thermal nonlinearity as peak and valley separation, i.e., $z_R > 1.7\,z_0$, and cw laser is used [34]. Nonlinear absorption in thin films was studied by open-aperture Z-scan shown in Fig. 7. All curves exhibit dip in the transmittance at the focus indicating the occurrence of reverse saturable absorption (RSA). It is found that thin film of all composite samples shows very large value of β for the given laser excitation. The coefficient of absorption attains maximum value for 5 wt% Cd–CuO–PVA thin film. The enhancement in the nonlinear coefficient in the present case may be explained on the basis of strong linear absorption coefficient combined with increased thermo-optic coefficient. In case of these doped thin film nanocomposites, nonlinear refractive index may not be purely dependent on coefficient of linear absorption which is decreasing as the concentration of Cd doping increases. For these composite thin films, the ratio α/D (or α/κ) is more important, and this ratio must be increasing in the present case. Although, in case of doped CuO NPs, linear absorption coefficient (α) is not considerably increasing with increase in doping concentration, other mechanisms originating in thin film composite structure may provide stimulus for the linear absorption. Doping into NPs may result additional local polarizability and anharmonicity creating interacting phonon subsystems [37]. The interaction of these phonon subsystems with incident light beam may show piezooptical or photoelastic effect and contribute toward the enhancement of second-order and third-order nonlinear optical properties [38]. The presence of polymeric host material (PVA) with different dielectric constant also plays an important role in determining NLO properties of the colloidal system due to dielectric effects and surface states effects [39, 40]. The values of n_2, β and other important NLO parameters such as real and imaginary parts of third-order NLO susceptibility and effective third-order NLO susceptibility are calculated and are listed in Table 3.

4 Conclusions

In conclusion, we report synthesis of L-arginine surface-modified CuO nanoparticles (NPs) doped with Cd and Cd–CuO–PVA nanocomposite thin films by spin coating method. Linear optical properties have been studied with ultraviolet–visible (UV–Vis) spectroscopy which attests the formation of CuO NPs by witnessing strong blue shift in the excitonic absorption from 365 to 342 nm. X-ray diffraction (XRD) shows formation of crystalline CuO having monoclinic phase with average particle size of 10 nm. Both XRD and UV–Vis data confirm decrease in particle size with increase in Cd-doping concentration. Fourier transform infrared (FTIR) spectra confirm the role of L-arginine as capping agent. Thin films and NPs have also been characterized by transmission electron microscopy (TEM), field emission scanning electron microscopy (FESEM) and energy-dispersive X-ray absorption (EDX) spectroscopy. Thin films have been characterized by Z-scan technique under continuous-wave (cw) He–Ne laser, and enhanced values of nonlinear refractive index n_2 and nonlinear absorption coefficient β have been obtained. Enhancements in the nonlinear optical properties have been attributed to the thermal effect due to strong linear absorption coefficient combined with increased thermo-optic coefficient.

Fig. 7 Closed- and open-aperture Z-scan curves for thin film samples
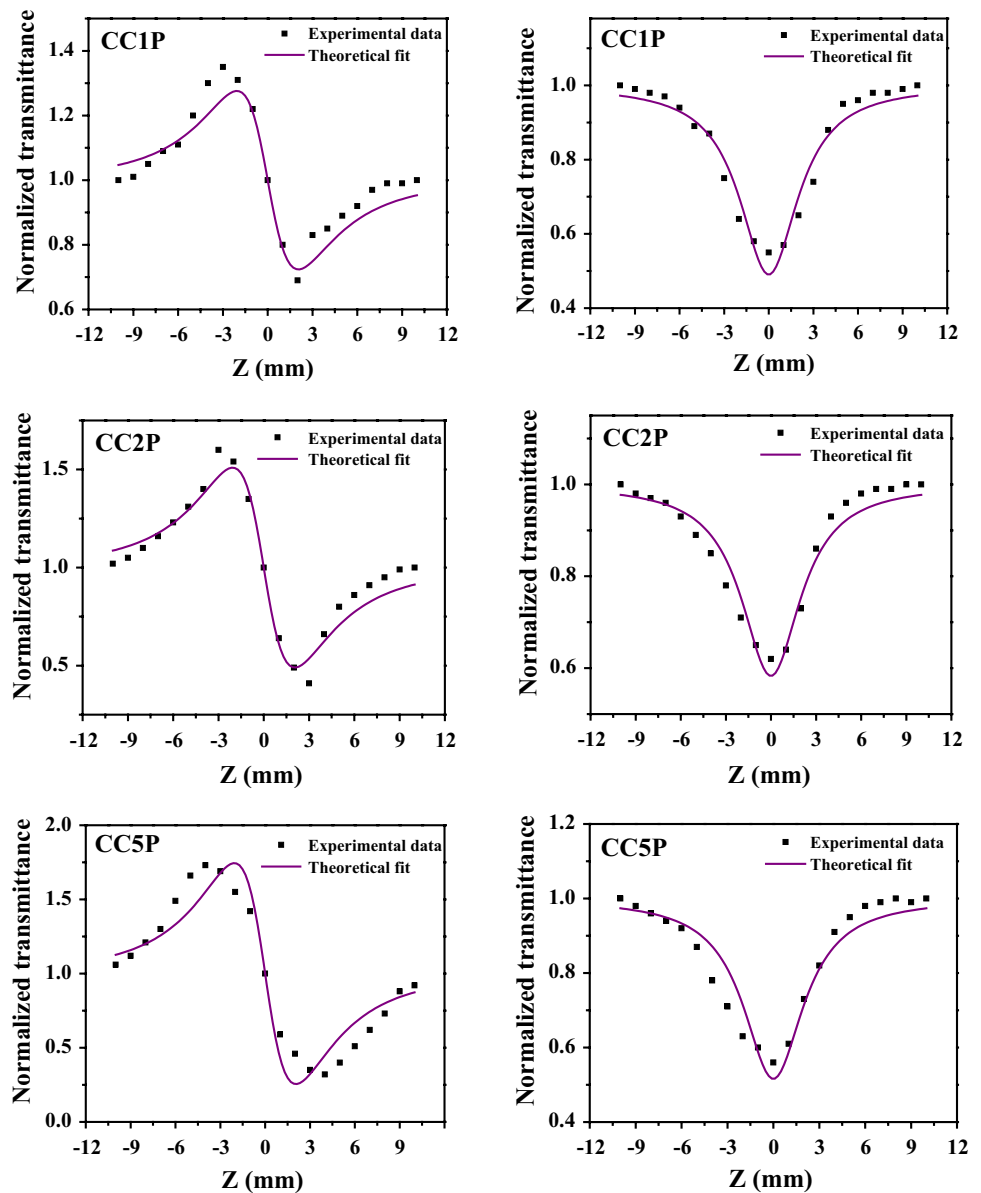
Table 3 Nonlinear optical coefficients obtained for thin film samples

Thin film samples	Nonlinear refractive index, n_2 (cm²/W) ($\times 10^{-5}$)	Nonlinear absorption coefficient, β (cm/W) ($\times 10^{-6}$)	Re[$\chi^{(3)}$] esu ($\times 10^{-3}$)	Im[$\chi^{(3)}$] esu ($\times 10^{-9}$)	$\chi^{(3)}$ esu ($\times 10^{-3}$)
CLP	18.6	1.60	32.6	0.82	32.6
CC1P	19.2	8.96	33.6	5.64	33.6
CC2P	35.8	10.4	62.7	4.62	62.7
CC5P	38.9	11.0	68.2	5.36	68.2

References

1. X. Zhong, R. Xie, Y. Zhang, T. Basche, W. Knoll, High-quality violet-to red-emitting ZnSe/CdSe core/shell nanocrystals. Chem. Mater. **17**, 4038 (2005)

2. H. Zhong, Y. Zhou, Y. Yang, C. Yang, Y. Li, Synthesis of type II CdTe-CdSe nanocrystal heterostructured multiple-branched rods and their photovoltaic applications. J. Phys. Chem. C **111**, 6538 (2007)

3. C.Y. Zhang, H.C. Yeh, M.T. Kuroki, T.H. Wang, Single-quantum-dot-based DNA nanosensor. Nat. Mater. **4**, 826 (2005)

4. R. Agarwal, C.M. Lieber, Semiconductor nanowires: optics and optoelectronics. Appl. Phys. A Mater. Sci. Process. **85**, 209 (2006)

5. L. Guo, S. Yang, C. Yang, P. Yu, J. Wang, W. Ge, G.K. Wong, Highly monodisperse polymer-capped ZnO nanoparticles: preparation and optical properties. Appl. Phys. Lett. **76**, 2901 (2000)

6. S.J. Mathews, S.C. Kumar, L. Giribabu, S.V. Rao, Large third-order optical nonlinearity and optical limiting in symmetric and unsymmetrical phthalocyanines studied using Z-scan. Opt. Commun. **280**, 206–212 (2007)

7. D.I. Kovsh, D.J. Hagan, E.W. Van Stryland, Numerical modeling of thermal refraction in liquids in the transient regime. Opt. Express **4**(8), 316 (1999)

8. R.K. Swarnkar, S.C. Singh, R. Gopal, Synthesis of copper/copper-oxide nanoparticles: optical and structural characterizations. AIP Conf. Proc. **1147**, 205 (2009)

9. K. Santra, C.K. Sarkar, M.K. Mukherjee, Copper oxide thin films grown by plasma evaporation method. Thin Solid Films **213**, 226 (1992)

10. J. Zhang, J. Liu, Q. Peng, X. Wang, Y. Li, Nearly monodisperse Cu_2O and CuO nanospheres: preparation and applications for sensitive gas sensors. Chem. Mater. **18**, 867 (2006)

11. A.H. MacDonald, Superconductivity: copper oxides get charged up. Nature **414**, 409 (2001)

12. R.V. Kumar, Y. Diamant, A. Gedanken, Sonochemical synthesis and characterization of nanometer-size transition metal oxides from metal acetates. Chem. Mater. **12**, 2301 (2000)

13. F. Lanza, R. Feduzi, J.J. Fuger, Effects of lithium oxide on the electrical properties of CuO at low temperatures. J. Mater. Res. **5**, 1739 (1990)

14. X.P. Gao, J.L. Bao, G.L. Pan, H.Y. Zhu, P.X. Huang, F. Wu, D.Y. Song, Preparation and electrochemical performance of polycrystalline and single crystalline CuO nanorods as anode materials for Li ion battery. J. Phys. Chem. B **108**, 5547 (2004)

15. O.G.M. Saavedra, L. Castaneda, J.G. Banuelos, R.O. Martinez, Laser Phys. **18**, 283 (2008)

16. U. Newmann, R. Grunwald, U. Griedner, G. Steinmeyer, Second-harmonic efficiency of ZnO nanolayers. Appl. Phys. Lett. **84**, 170 (2004)

17. Y.S. Tamgadge, A.L. Sunatkari, S.S. Talwatkar, V.G. Pahurkar, G.G. Muley, Linear and nonlinear optical properties of nanostructured $Zn_{(1-x)}Sr_xO$-PVA composite thin films. Opt. Mater. **37**, 42–50 (2014)

18. S.S. Talwatkar, Y.S. Tamgadge, A.L. Sunatkari, A.B. Gambhire, G.G. Muley, Amino acids (L-arginine and L-alanine) passivated CdS nanoparticles: synthesis of spherical hierarchical structure and nonlinear optical properties. Solid State Sci. **38**, 42–48 (2014)

19. S.S. Talwatkar, A.L. Sunatkari, Y.S. Tamgadge, V.G. Pahurkar, G.G. Muley, Influence of Li^+ and Nd^{3+} co-doping on structural and optical properties of L-arginine-passivated ZnS nanoparticles. Appl. Phys. A **118**, 675–682 (2015)

20. M. Sheik-Bahae, A.A. Said, E.W. Van Stryland, High-sensitivity, single-beam n_2 measurements. Opt. Lett. **14**, 955–957 (1989)

21. M. Sheik-Bahae, A.A. Said, T.H. Wei, D.J. Hagan, E.W. Van Stryland, Sensitive measurement of optical nonlinearities using a single beam. IEEE J. Quantum Electron. **26**, 760–769 (1990)

22. Hui Wang, Xu Jin-Zhong, Jun-Jie Zhu, Hong-Yuan Chen, Preparation of CuO nanoparticles by microwave irradiation. J. Cryst. Growth **244**, 88–94 (2002)

23. K. Borgohain, S. Mahamuni, Formation of single-phase CuO quantum particles. J. Mater. Res. **17**, 1220–1223 (2002)

24. C. Schmid, *Nanoparticles*, 1st edn. (Wiley, Weinheim, 2004)

25. J.I. Pankove, *Optical Processes in Semiconductors* (Dover, New York, 1971)

26. B.L. Justus, M.E. Seaver, J.A. Ruller, A.J. Campillo, Excitonic optical nonlinearity in quantum-confined CuCl-doped borosilicate glass. Appl. Phys. Lett. **57**, 1381 (1990)

27. E. Hanamura, Rapid radiative decay and enhanced optical nonlinearity of excitons in a quantum well. Phys. Rev. B **37**, 1273 (1988)

28. L.E. Brus, Electronic wave functions in semiconductor clusters: experiment and theory. J. Phys. Chem. **90**, 2555 (1986)

29. A.M. Petrosyan, R.P. Sukiasyan, Vibrational spectra of L-arginine nitrates. J. Mol. Struct. **874**, 51–56 (2008)

30. H. Hagemann, H. Bill, W. Sadowski, E. Walker, M. Francois, Raman spectra of single crystal CuO. Solid State Commun. **73**, 447 (1990)

31. G. Kliche, Z.V. Popovic, Far-infrared spectroscopic investigations on CuO. Phys. Rev. B **42**, 10060 (1990)

32. P.Y. Yu, Y.R. Shen, Study of photoluminescence in Cu_2O. Phys. Rev. B **12**, 1377 (1975)

33. B.D. Cullity, *Elements of X-Ray Diffraction*, 2nd edn. (Addison-Wesley, Reading, 1956)

34. R.W. Boyd, *Nonlinear Optics*, 3rd edn. (Elsevier, Burlington, 2008)

35. J.P. Gorden, R.C.C. Leite, R.S. Moore, S.P.S. Porto, R. Whinner, Long-transient effects in lasers with inserted liquid samples. J. Appl. Phys. **36**, 3–8 (1965)

36. De Nalda et al., Limits to the determination of the nonlinear refractive index by the Z-scan method. J. Opt. Soc. Am. B **19**, 289 (2002)

37. T.M. Williams, D. Hunter, A.K. Pradhan, I.V. Kityk, Photoinduced piezo-optical effect in Er doped ZnO films. Appl. Phys. Lett. **89**, 043116 (2006)

38. J. Ebothe, W. Gruhn, A. Elchichou, I.V. Kityk, R. Dounia, M. Addou, Giant piezooptics effect in the ZnO–Er^{3+} crystalline films deposited on the glasses. Opt. Laser Technol. **36**, 173 (2004)

39. J. Ebothe, R. Miedzinski, V. Kapustianyk, B. Turko et al., Optical SHG for ZnO films with different morphology stimulated by UV-laser thermotreatment. J. Phys. Conf. Ser. **79**, 012001 (2007)

40. J.Z. Zhang, *Optical Properties and Spectroscopy of Nanomaterials* (World Scientific, Singapore, 2009)